

Structural, morphological, optical and opto-thermal properties of Ni-doped ZnO thin films using spray pyrolysis chemical technique

S RAJEH¹, A BARHOUMI¹, A MHAMDI^{2,*}, G LEROY³, B DUPONCHEL⁴, M AMLOUK²
and S GUERMAZI¹

¹Unit of Physics of Insulators Materials and Semi-insulators, Sfax University, B.P. 1171, 3000 Sfax, Tunisia

²Unité de physique des dispositifs à semi-conducteurs, Tunis El Manar University, 2092 Tunis, Tunisia

³University Lille North of France, ULCO, UDSMM, 62228 Calais, France

⁴University Lille North of France, ULCO, UDSMM, 59140 Dunkerque, France

MS received 21 September 2014; accepted 6 July 2015

Abstract. Nickel-doped zinc oxide thin films (ZnO : Ni) at different percentages were deposited on glass substrates using a chemical spray technique. The effect of Ni concentration on the structural, morphological, optical and photoluminescence (PL) properties of the ZnO : Ni thin films were investigated. X-ray diffraction analysis revealed that all films consist of single phase ZnO and was well crystallized in würtzite phase with the crystallites preferentially oriented towards the (002) direction parallel to the *c*-axis. The optical transmittance measurement was found to be higher than 90%, the optical band gap values of ZnO thin films decreased after doping from 3.29 to 3.21 eV. A noticeable change in optical constants was observed between undoped and Ni-doped ZnO. Room-temperature PL is observed for ZnO, and Ni-doped ZnO thin films.

Keywords. Thin films; Ni-doped ZnO; chemical spray; optical properties; photoluminescence; opto-thermal.

1. Introduction

Zinc oxide (ZnO) is a wide band gap semiconductor with an energy gap of 3.37 eV at room temperature. As a consequence, ZnO absorbs UV radiation because of band-to-band transitions. It has been used considerably for semiconducting multilayers [1], photothermal conversion system [2], photocatalytic [3], solar cells [4], gas sensors [5] and transparent electrodes [6]. Among all the oxide materials studied, in the last years, ZnO emerged as one of the most promising materials owing to its optical and electrical properties, high chemical and mechanical stabilities, together with its abundance in nature, which makes it a lower cost material when compared with the most currently used transparent conductive oxide materials (ITO and SnO₂).

Many methods have been described in the literature for the production of ZnO thin films such as sputtering [7,8], thermal evaporation [9], and spray pyrolysis [10] were applied for the production of ZnO. Spray pyrolysis technique is preferred among these techniques since it is cheaper, simpler and more versatile than the others, which allows the possibility of obtaining films with the required properties for different applications as well as large area films.

The n-type semiconductor behaviour is originated by the ionization of excess zinc atoms at interstitial positions and the oxygen vacancies [11]. It is well known that the addition of dopants into a wide gap semiconductor, such as ZnO, can often induce dramatic changes in the optical, electrical

and magnetic properties [10,12]. Transition metal elements have been successfully employed as dopants in ZnO such as V, Cu, Mn and Ni [13–16]. Ni is an important dopant in the magnetic materials [17–19]. Furthermore, Ni²⁺ (0.69 Å) has the same valence compared with Zn²⁺ and its radius is close to Zn²⁺ (0.74 Å), so it is possible for Ni²⁺ to replace Zn²⁺ in ZnO lattice. Some research works on Ni-doped ZnO showed that the luminescence properties of ZnO changed after doping of Ni [20–23].

In this paper, the influence of Ni doping on the structural, morphological, optical and photoluminescence (PL) properties of ZnO films is reported.

2. Experimental

Ni-doped ZnO thin films deposited on glass substrates were prepared by the spray pyrolysis technique. Undoped ZnO thin films were prepared using zinc acetate (C₄H₆O₄Zn·2H₂O) dissolved in isopropyl alcohol to obtain a starting solution with a 10⁻¹ mol l⁻¹ concentration.

Doping of ZnO thin films with nickel was carried out by adding the compound source of Ni (NiCl₂) in the starting solution with an atomic percentage [Ni/Zn] = 2, 3 and 4 at. wt%. The resulting solution was stirred at 100°C for 20 min to lead to a clear and homogeneous solution. Glass slides (2 cm × 1 cm) were used as substrates. Before loading into the system, the substrates were washed with detergent and then completely rinsed in methanol, acetone and finally dried in air. Then the substrates were progressively heated up to the

*Author for correspondence (mhaammar@gmail.com)

required temperature, before being sprayed on. The deposition temperature T_s (temperature at the substrate surface) was maintained at 460°C.

The structure and the crystallinity of the ZnO and Ni-doped ZnO thin films were determined by a copper-source diffractometer (Analytical X Pert PROMPD), with the wavelength $\lambda = 1.54056 \text{ \AA}$. The surface morphology of the films was examined by atomic force microscopy (AFM) and scanning electron microscopy (SEM). AFM experiments were conducted on a Veeco (now Brükker) multimode used in contact mode and SEM observations on a Quanta 200 FEI at 15 and 25 kV. In order to determine band gap energy and optical constants of ZnO and Ni-doped ZnO in thin films, the optical transmission and absorption were studied in the wavelength range of 200–3000 nm, using a Shimadzu UV3101 PC spectrophotometer.

3. Results and discussion

3.1 Structural properties

The crystal structures of undoped and Ni-doped ZnO were studied by means of X-ray diffraction (XRD). Figure 1 shows

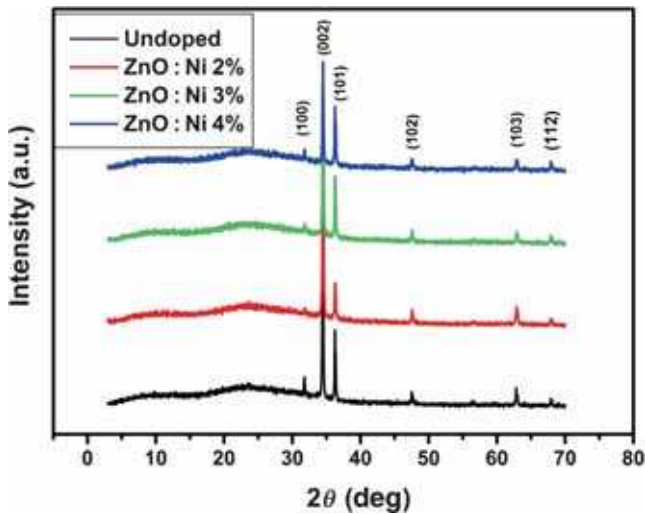


Figure 1. XRD patterns of undoped and Ni-doped sprayed ZnO thin layers.

the XRD patterns of undoped and Ni-doped ZnO. The XRD patterns of these samples are in good agreement with the Joint Committee on Powder Diffraction Standards (JCPDS) (No. 36-1451) data of wurtzite (hexagonal) ZnO powder. It is observed that undoped and Ni-doped ZnO samples exhibit peaks corresponding to the (100), (002), (101), (102), (103) and (112) planes, with the (002) peak showing the highest intensity in all cases, implying that all the samples have a hexagonal crystal structure with a preferred orientation with the substrate normal parallel to the normal of the ZnO (002) plane. The diffraction peaks attributed to Ni-related secondary phases have not been observed. In addition, the position of the (002) peak shifted slightly ($\approx 0.03^\circ$) from $2\theta = 34.45^\circ$ in undoped ZnO film to higher angles as Ni content increases ($2\theta = 34.48^\circ$ for ZnO : Ni 4%), indicating that Ni ions substitute Zn ions in the ZnO lattice owing to the slight difference between the ionic radii of Ni^{2+} (0.069 Å) and Zn^{2+} (0.74 Å) [24].

The lattice constants can be calculated using the following relation [25]:

$$\frac{1}{d_{hkl}^2} = \frac{4}{3} \left(\frac{h^2 + hk + k^2}{a^2} \right) + \frac{l^2}{c^2}, \quad (1)$$

where a and c are the lattice constants and d_{hkl} the crystalline surface distance for hkl indices. Table 1 lists the calculated values of d_{hkl} and lattice parameters of undoped and Ni-doped ZnO thin films. It is observed that d_{hkl} values are in good agreement with those reported in JCPDS data cards (No. 36–1451). It can be seen that the interplanar spacing d_{hkl} values decrease with Ni content. This phenomenon shows that Ni element used at lower concentrations is introduced in the ZnO matrix and played an important role in improving the transparency of such doped films [26].

The average crystallite size of undoped and Ni-doped ZnO is estimated from (002) principal peak by using the Debye–Scherrer formula [27]:

$$D = \frac{H\lambda}{\beta \cos \theta}, \quad (2)$$

where $\lambda = 1.5418 \text{ \AA}$ for Cu radiation, θ is the diffraction angle, $K = 0.9$ and β the full-width at half-maximum (FWHM) with $\beta = \sqrt{\beta_c^2 - \beta_0^2}$, where β_c is measured from

Table 1. Position of the (002) peak and some relevant parameters.

	Results JCPDS (pure powder ZnO)	Experiment : Ni content Ni/ Z_n (%)			
		0	2	3	4
The position of (002) peak in 2θ (deg)		34.454	34.479	34.489	34.484
Interplanar spacing d_{hkl} (Å)	(002)	2.602	2.603	2.601	2.600
	(101)	2.476	2.478	2.476	2.478
a (Å)		3.249	3.254	3.252	3.254
c (Å)		5.205	5.206	5.202	5.202
c/a		1.602	1.600	1.599	1.598

the film and β_0 corresponds to the reference powder [27,28]. The results are shown in table 2. As the concentration of Ni increases, an increase in the crystallite size is observed. The same behaviour is reported by the Muniyandi *et al* [29] in a study on Ni-doped ZnO prepared by the spray pyrolysis deposition technique. Muniyandi *et al* found that the crystallite size increase with the increase in Ni concentration might be due to the agglomeration. This has been further confirmed by the decrease in the value of lattice parameter c .

Additional information on structural properties can be obtained from the residual stress measurements calculated by [30].

$$\sigma = 450 \frac{c_0 - c}{c_0}, \quad (3)$$

where σ (in GPa) is the mean stress, c the lattice constant of ZnO thin films and c_0 the lattice constant of the bulk material (standard $c_0 = 0.5206$ nm). The calculated data are summarized in table 2. A slight deviation of the (002) peak was revealed when the concentration varied. This indicates that some residual stress inside the film is occurring.

In the same line, the microstrain in these thin films was calculated with the following relation:

$$\varepsilon_s = \frac{\beta \cos \theta}{4}, \quad (4)$$

where θ is the (002) diffraction angle. It is noticed that the microstrain of the films decreased when the concentration of Ni increased (see table 2). This is probably due to the ionic radius of Zn^{2+} which is higher compared with that of Ni^{2+} [31].

The preferred orientations of the Ni-doped ZnO thin films are evaluated by the texture coefficient (TC), calculated from the X-ray data using the well-known formula

$$\text{TC}(hkl) = \frac{I(hkl)/I_0(hkl)}{1/N \sum_{hkl} I(hkl)/I_0(hkl)}, \quad (5)$$

where $\text{TC}(hkl)$ is the texture coefficient of the hkl planes, $I(hkl)$ is the measured or normalized intensity of a plane (hkl), I_0 the corresponding standard intensity given in JCPDS data, N the number of reflections and n the number of diffraction peaks. The value of TC calculated for the diffraction peaks (002) and (101) of all samples are shown in

table 2. From these results, it is observed that TC(002) is so high, showing that the crystallites are mainly perpendicular to substrate plane (parallel to the c -axis) for ZnO undoped and doped thin films.

3.2 Surface morphology

The surface morphology of undoped and Ni-doped ZnO thin films was characterized by AFM and SEM. Figure 2 shows the typical SEM images of the ZnO and Ni-doped ZnO thin films. It is seen grains of about 100 nm of diameter nearby large plates of several hundred nanometers long. The three-dimensional (3D) images of AFM micrographs are shown in figure 3. According to them, grains are clearly spherical and the large plates seen with the SEM seem to be agglomerates of grains. On the AFM pictures, grains appear wider than on SEM images. It is a normal probe-based artefact when measuring globular features. All the films exhibit spherical grains, indicating the polycrystalline nature of these films. The SEM micrographs also reveal that Ni doping ZnO thin films can increase the average grain size, this result agrees with XRD measurements. The same behaviour is reported by the Muniyandi *et al* in a study on Ni-doped ZnO prepared by the spray pyrolysis deposition technique [29].

In addition, AFM was used to measure the surface roughness of the films over a $2 \mu\text{m} \times 2 \mu\text{m}$ area. The root-mean squares (RMS) roughness of undoped and Ni-doped ZnO thin films ($[\text{Ni}]/[\text{Zn}] = 0, 0.02, 0.03$ and 0.04) are determined as 28.95; 28.98; 32.30 and 36.63 nm, respectively. As the $[\text{Ni}]/[\text{Zn}]$ ratio increases, the surface roughness increases as a result of grains increasing caused by the Ni doping and grains agglomeration.

Morphological study reveals that the percentage of dopant has an influence on the morphology and the roughness of the films. However, a slightly tormented surface is quite favourable for the use of such component type in the photovoltaic conversion field.

3.3 Optical study

3.3a Optical band-gap: In order to correlate the optical behaviour of films with structural and morphological results, the optical transmittance of samples has been investigated in the wavelength range of 200–3000 nm using UV–vis

Table 2. Crystallite size (D), texture coefficient (TC), stress (σ) and microstrain (ε_s) of the sprayed Ni-doped ZnO thin films.

Samples	ZnO	ZnO : Ni 2%	ZnO : Ni 3%	ZnO : Ni 4%
Peak width at mid-height β (deg)	0.1021	0.0836	0.0771	0.0669
The grain size D (nm)	81.61	99.57	108.11	124
σ (GPa)	0	0.345	0.432	0.345
ε_s (10^{-4})	4.250	3.483	3.212	2.787
TC (002)	4.727	4.401	4.744	3.894
TC (101)	0.802	0.331	0.737	0.941

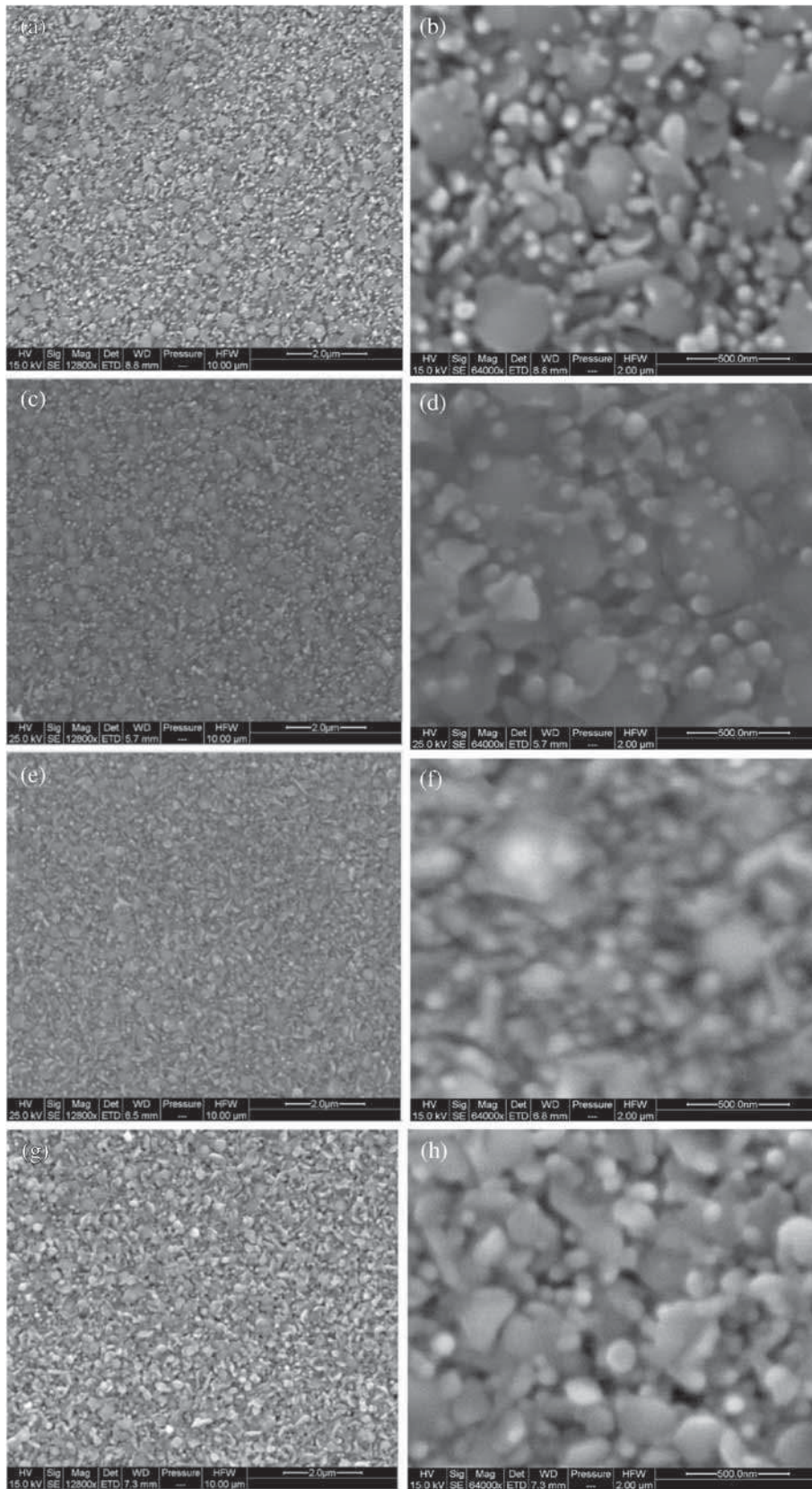


Figure 2. SEM images of pure and Ni-doped ZnO thin films at low magnification and at high magnification: (a, b) ZnO, (c, d) ZnO : Ni 2%, (e, f) ZnO : Ni 3% and (g, h) ZnO : Ni 4%.

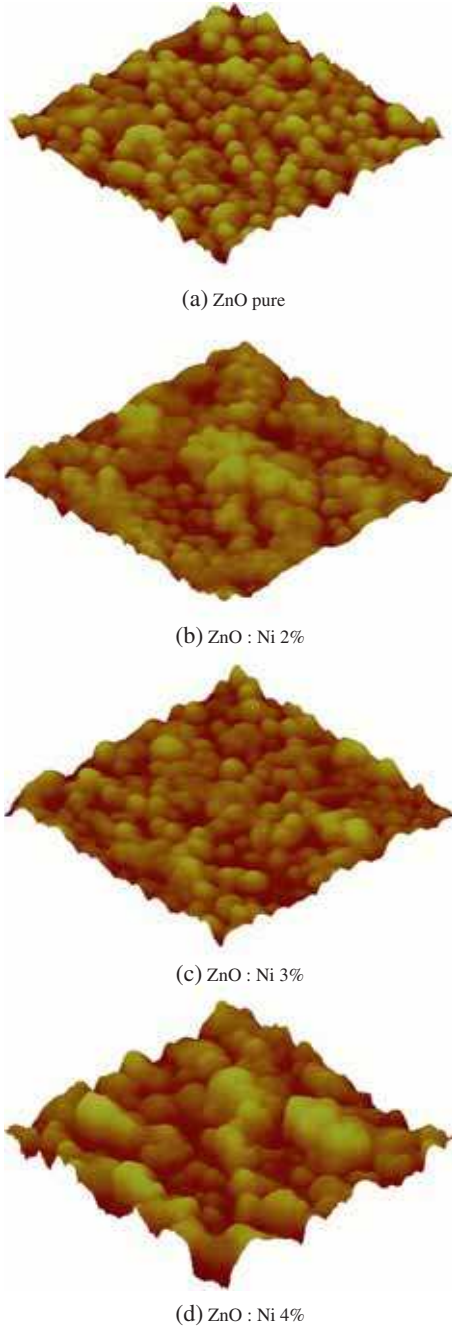


Figure 3. AFM 3D micrographs of sprayed ZnO : Ni thin films: (a) ZnO, (b) ZnO : Ni 2%, (c) ZnO : Ni 3% and (d) ZnO : Ni 4%. Scan area: $2 \mu\text{m} \times 2 \mu\text{m}$. Vertical range: 500 nm.

spectroscopy (figure 4). It is clear from figure 4 that all the samples exhibit a high transmittance around 85% for $\lambda > 625 \text{ nm}$. Some interference fringes appear on all spectra. They are due to multiple reflections from the both sides of the film. From figure 4, it is deduced that all the samples have sharp absorption edges in the wavelength region between 360 and 400 nm. The absorption edge of Ni-doped ZnO films deposited for different doping concentrations shifts to a larger wavelength. This phenomenon indicates that the optical energy gap decreases with doping concentration. It is well

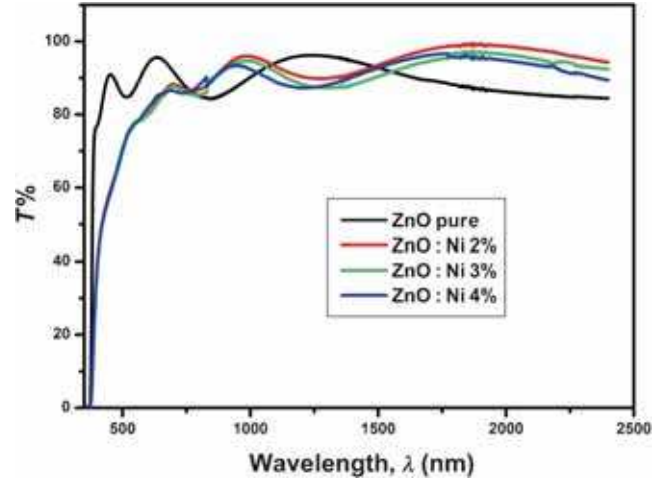


Figure 4. Transmission spectra of sprayed ZnO : Ni thin films.

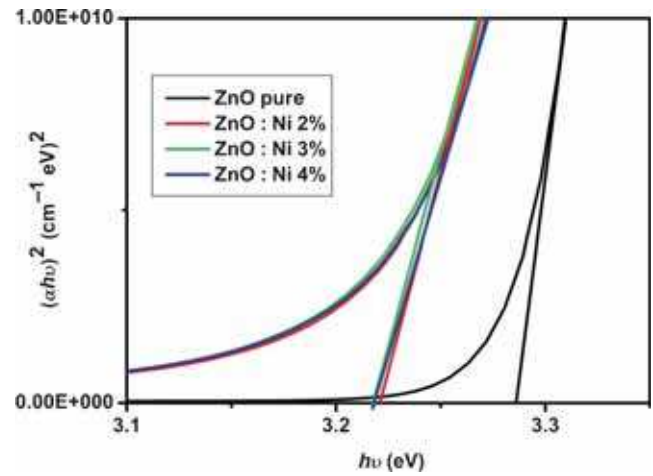


Figure 5. Variation of the absorption as a function of the light energy of sprayed ZnO : Ni thin films.

known that the theory of optical absorption gives the relation between absorption coefficients α and photon energy $h\nu$ for direct allowed transition as [32].

$$\alpha h\nu = [A (h\nu - E_g)]^{1/2}, \quad (6)$$

where A is a constant, E_g the optical band gap energy, $h\nu$ is the photon energy and α the absorption coefficient. The band gap is determined using this equation when the straight portion of $(\alpha h\nu)^2$ against $h\nu$ plot is extrapolated to intersect the energy axis at zero. Graph of $(\alpha h\nu)^2$ vs. $h\nu$ for ZnO and for different Ni concentrations in ZnO is shown in figure 5. The obtained band gaps of un-doped ZnO, ZnO : Ni 2%, ZnO : Ni 3% and ZnO : Ni 4% thin films are 3.29, 3.22, 3.21 and 3.21 eV, respectively. It can be seen also that the value of E_g of Ni-doped ZnO decrease when Ni concentration increases. It might be due to the increase in the grain size [33] as well as due to the lowering of the conduction band induced by donor level created by the Ni defects [34].

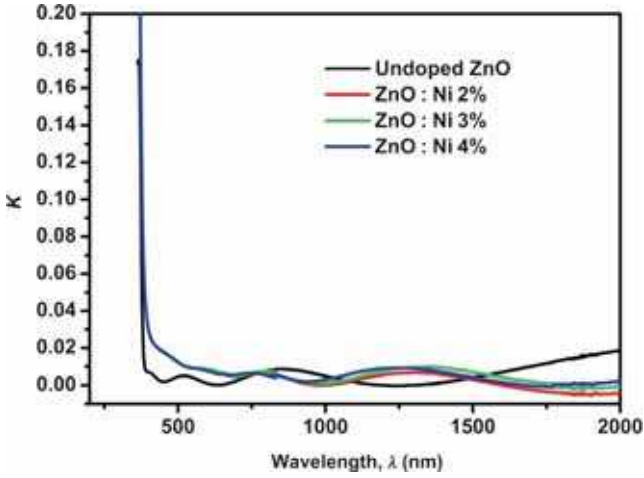


Figure 6. Extinction coefficient k of sprayed ZnO : Ni thin films.

3.3b *Refractive index and extinction coefficient:* The extinction coefficient $k(\lambda)$ of undoped and Ni-doped ZnO thin films (figure 6), was calculated using the following expression [35]:

$$k = \frac{\alpha\lambda}{4\pi}. \quad (7)$$

The refractive index $n(\lambda)$ can be determined by using the envelopes of the transmittance $T(\lambda)$ of thin films deposited on a transparent substrate. The method of envelopes implies that the glass substrate is transparent [36]. The refractive index $n(\lambda)$ for various wavelengths and for curves envelopes T_M (for the maximum values of transmittance) and T_m (for the minimum values) is expressed by [37,38]:

$$n = \left[N + (N^2 - S^2)^{1/2} \right]^{1/2}, \quad (8)$$

where

$$N = 2S \frac{T_M - T_m}{T_M T_m} + \frac{s^2 + 1}{2}. \quad (9)$$

Here, S is the refractive index of the glass substrate. Figure 7 shows the refractive index n for the undoped and Ni-doped ZnO thin films as a function of wavelength. The values of both n and k decrease with the increase in wavelength of the incident photon. In addition, the high values of k in the fundamental absorption region (low wavelength $\lambda < 400$ nm) are due to the intrinsic absorption for the higher energy gap. In the visible, the low values of k imply that these layers are transparent as showed in the transmission spectra. It should be mentioned that in the wavelength range of 400–800 nm, the refractive index exhibits a normal dispersion and the extinction coefficient k value is very low, the later confirming that of all the films studied in this work are homogeneous and highly transparent. A dependence on wavelength of the refractive index and the extinction coefficient with the doping concentration is observed. This phenomenon can be explained on the basis of the contribution from both lattice

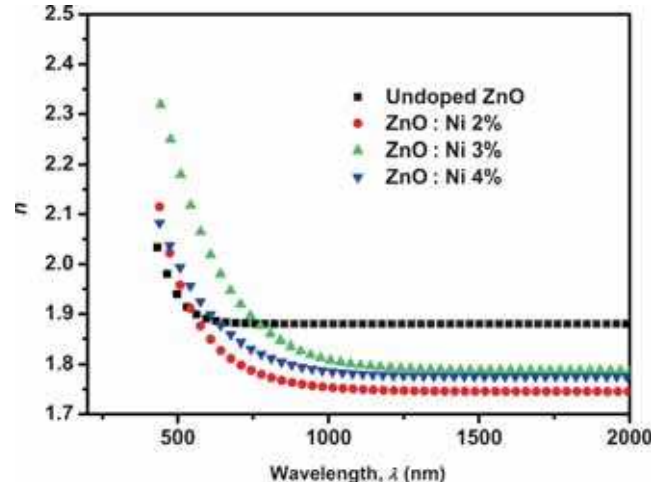


Figure 7. Refractive index n of sprayed ZnO : Ni thin films.

parameter change and the presence of defaults in the prepared films.

Owing to its straightforward link with the dispersion energy, the refractive index $n(\lambda)$ remains an important physical property of materials dedicated to optical devices. In order to achieve a better understanding of the refractive index dispersion of the Ni-doped ZnO thin films, $n(\lambda)$ was analysed by the single oscillator model proposed by Wemple and DiDomenico [39–42]. In this model, in the region of low absorption the photon energy dependence of the refractive index n is expressed by

$$n^2 = 1 + \frac{E_0 E_d}{E_0^2 - (h\nu)^2}, \quad (10)$$

where E_0 is the single oscillator energy and E_d the dispersion energy corresponding to the average strength of the inter-band optical transitions. E_0 and E_d are therefore determined through a linear fit of the plot of $1/(n^2 - 1)$ as a function of $(h\nu)^2$ (figure 8). The slope is $(E_0 E_d)^{-1}$ and the intercept with the zero photon energy axis gives (E_0/E_d) . The values of E_0 and E_d are reported in table 3 for all the films. Under the same model, the refractive index can also be analysed to determine the long wavelength refractive index n_∞ , average oscillator wavelength λ_0 and oscillator length strength S_0 of each thin film. These values can be obtained by using the following relations [43,44]:

$$\frac{n_\infty^2 - 1}{n^2 - 1} = 1 - \left(\frac{\lambda_0}{\lambda} \right)^2, \quad (11)$$

$$n_\infty^2 = 1 + S_0 \lambda_0^2, \quad (12)$$

$$n^2 - 1 = \frac{S_0 \lambda_0^2}{1 - (\lambda_0/\lambda)^2}, \quad (13)$$

n_∞ , S_0 and λ_0 values are obtained from the linear of $1/(n^2 - 1)$ vs. λ^{-2} and are given in table 3. It is found that, the nickel doping decreases the refractive index, n_0 and ε_∞ for all films.

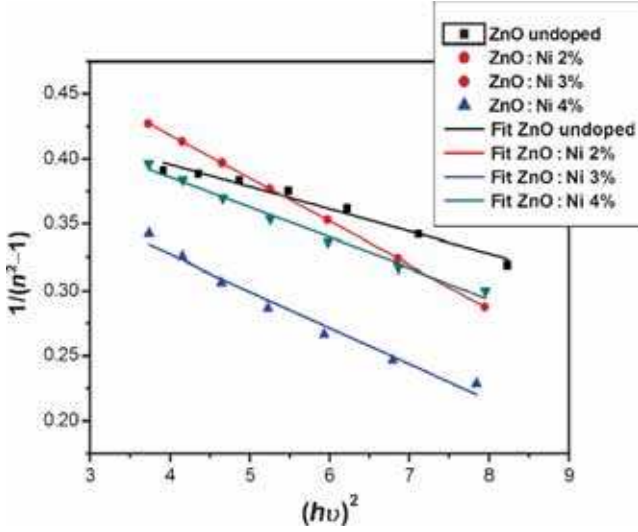


Figure 8. A plot of $(n^2-1)^{-1}$ vs. photon energy squared $(h\nu)^2$ of sprayed ZnO : Ni thin films.

Table 3. Calculated values of E_0 , E_d and other constants.

Samples	E_d (eV)	E_0 (eV)	λ_0 (μm)	S_0 (μm^{-2})	n_∞
ZnO pure	7.713	3.780	0.328	18.965	1.743
ZnO : Ni 2%	7.687	4.194	0.295	20.971	1.683
ZnO : Ni 3%	7.976	3.815	0.325	19.791	1.758
ZnO : Ni 4%	8.949	4.446	0.278	25.875	1.735

3.3c Dielectric constant: The optical characteristics of undoped and Ni-doped ZnO are linked to its dielectric function too. The real $\varepsilon_1(\lambda)$ and the imaginary $\varepsilon_2(\lambda)$ parts of complex dielectric function are related to refractive index $n(\lambda)$ and extinction coefficient $k(\lambda)$ via the following relations [44,45]:

$$\varepsilon(\lambda) = (n(\lambda) - ik(\lambda))^2 = \varepsilon_1(\lambda) - i\varepsilon_2(\lambda), \quad (14)$$

$$\varepsilon_1(\lambda) = n(\lambda)^2 - k(\lambda)^2, \quad (15)$$

$$\varepsilon_2(\lambda) = 2n(\lambda)k(\lambda). \quad (16)$$

For all samples, it is found that in infrared range the dispersion of ε_1 is a linear function of the square of the wavelength λ^2 while the absorption ε_2 is a linear function of λ^3 (figure 9). This behaviour is in good agreement with the classical theory of the dielectric constant which is expressed by the following system in the near infrared ($\omega t \gg 1$) [46]:

$$\varepsilon_1 \approx \varepsilon_\infty - \frac{\varepsilon_\infty \omega_p^2}{4\pi^2 c^2} \lambda^2, \quad (17)$$

$$\varepsilon_2 \approx \varepsilon_\infty - \frac{\varepsilon_\infty \omega_p^2}{8\pi^3 c^3 \tau} \lambda^3, \quad (18)$$

where ε_∞ is the dielectric constant at high frequencies, ω_p the pulsation plasma and τ the relaxation time.

It can be seen that for all samples, in infrared range, ε_1 is a linear function of λ^2 while ε_2 is linear with λ^3 .

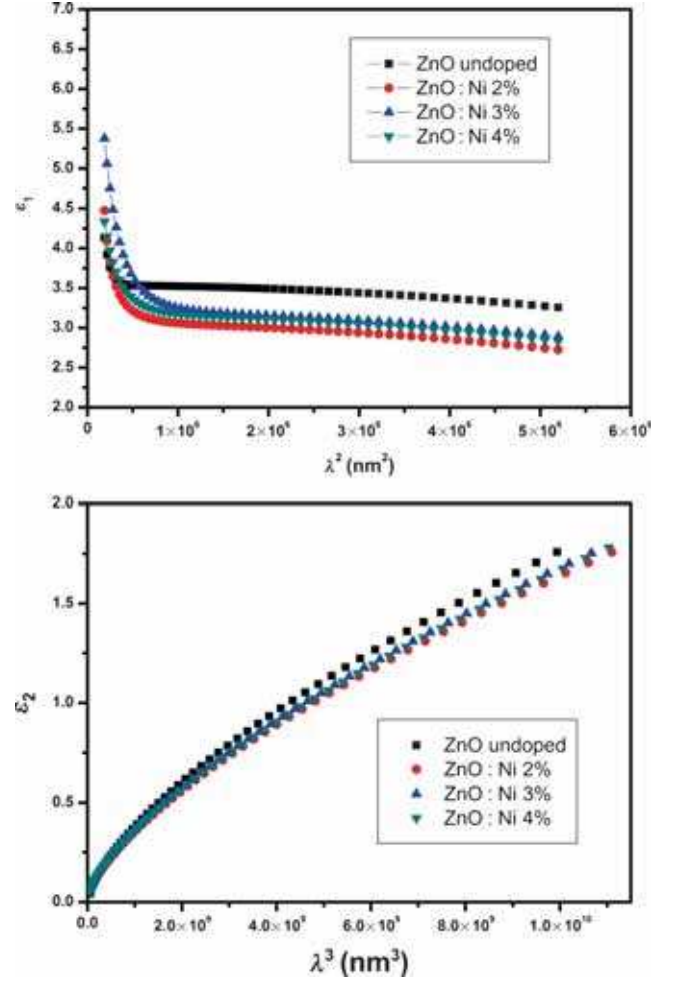


Figure 9. Variation of the real (ε_1) and imaginary (ε_2) parts and of dielectric constant of sprayed Ni-doped ZnO as a function of λ^2 and λ^3 , respectively.

These results can be used in order to determine the optical constants: ε_∞ , ω_p and τ which represent, respectively, the dielectric constant at high frequencies, the pulse plasma and the relaxation time which depends on the conduction mechanism of carriers in the optical and acoustic phonons, lattice defects and ionized impurities.

The free carrier's concentration-to-effective mass ratio N/m^* , is given from the system

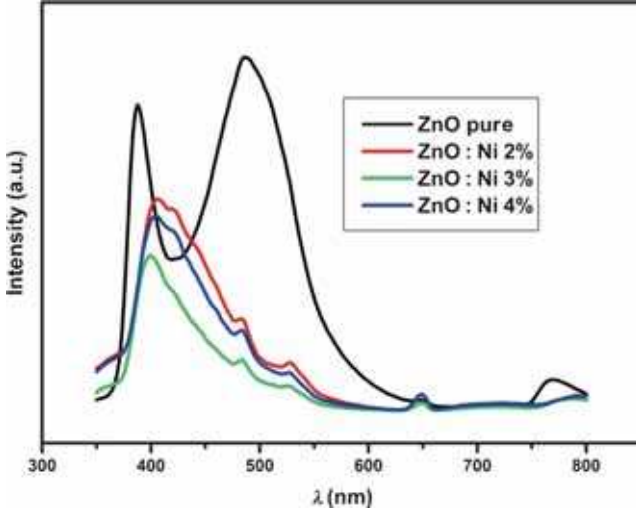
$$\omega_p^2 = \frac{4\pi N e^2}{\varepsilon_\infty m_e^*}. \quad (19)$$

The calculated values of these constants are listed in table 4.

3.3d Photoluminescence: PL measurement is a sensitive nondestructive way to study the intrinsic and extrinsic defects in semiconductor materials. It delivers abundant information on the energy states of impurities and defects, even at very low densities, which is helpful for understanding structural defects in semiconductors. Moreover, it provides an additional insight into the crystal quality of semiconductor

Table 4. Calculated values of ε_∞ , ω_p and other constants.

Samples	ε_∞	ω_p (10^{14} rad s $^{-1}$)	τ (10^{-14} s)	N/m^* (10^{17} g $^{-1}$ cm $^{-3}$)
ZnO pure	3.77	2.82	3.45	1.04
ZnO : Ni 2%	5.04	14.98	1.07	40.99
ZnO : Ni 3%	4.97	11.45	0.59	22.57
ZnO : Ni 4%	4.86	15.46	1.06	40.99

**Figure 10.** Room-temperature photoluminescence spectra of undoped and Ni-doped ZnO thin films.

films through different emissions. Figure 10 shows room-temperature PL spectra of undoped and Ni-doped ZnO thin films. A strong ultraviolet (UV) and blue-green emissions at around 387 and 488 nm are observed for undoped ZnO thin film. After Ni doping, the UV band emission shifts to 403 nm with the violet and blue-green emission bands are observed at 422, 484 and 528 nm, respectively.

The UV emission can be attributed to the near band edge (NBE) emission of ZnO and originated by the recombination of free exciton transition from the localized level below the conduction band to the valence band [47]. The band edge absorption peaks of Ni-doped ZnO thin films shifts to longer wavelengths (red shifted). Different authors have explained that the red shift in ZnO band edge absorption peak with transition metals doping can be assigned to sp–d spin exchange interactions between the band electrons of host matrix and the localized d-electrons of dopant ions substituting the cations [48–50]. They have discussed that s–d and p–d exchange interactions can give rise to negative and positive shifts to the conduction band and valence band edges, respectively, which leads to the narrowing of band gap. Hence, it can be concluded that Ni doping induced red shift in the band edge absorption peak of ZnO is due, in this case, to the sp–d exchange interactions. As the doping concentration increased the full-width half-maximum (FWHM) and the peak intensity of the UV emission decreased. Ni doping in ZnO causes creation of the defects, which might have

provided non-radiative pathways to limit the radiative efficiency of the films. The visible emission from undoped and Ni-doped ZnO thin films may be due to the defect, particularly the oxygen vacancy arising from the oxygen deficiency and both O and Zn interstitials [51]. A blue luminescence peak centred at 484 nm in visible region is observed for all the samples. The blue-green emission is caused by intrinsic defects and donor–acceptor pair recombination. Kohan *et al* [52] have calculated the energy levels of defects in ZnO thin films by a full-potential linear muffin-tin orbit method and shown that the energy interval between the Zn interstitial levels to the top of the valence band was about 2.9 eV. The luminescence centre (≈ 2.6 eV) calculated in this work agrees quite well with Kohan’s theoretical calculation. Therefore, the blue-green emission band is assigned to the electron transition from the Zn interstitial levels to the top of valence band. However, since the intensity of blue-green emission decreased in the nickel-doped samples it could be concluded that the defect states responsible for the broad blue-green emission in ZnO can be passivity by nickel.

3.4 Opto-thermal expansivity study

The Amlouk–Boubaker opto-thermal expansivity Ψ_{AB} is a thermo-physical parameter defined in precedent studies [53], as a 3D expansion velocity of the transmitted heat inside the material. It is expressed in m 3 s $^{-1}$, and calculated by

$$\Psi_{AB} = \frac{D}{\hat{\alpha}} \quad (20)$$

where D is the thermal diffusivity and $\hat{\alpha}$ the effective absorption, it is a weighted average of the absorption coefficient of the solar spectrum AM1.5. This parameter is shown as follows:

$$\hat{\alpha} = \frac{\int_0^1 I(\tilde{\lambda})_{AM1.5} \times \alpha(\tilde{\lambda}) d\tilde{\lambda}}{\int_0^1 I(\tilde{\lambda})_{AM1.5} d\tilde{\lambda}}, \quad (21)$$

$$\begin{cases} \lambda \in [\lambda_{\min}, \lambda_{\max}] \Leftrightarrow \tilde{\lambda} \in [0, 1], \\ \lambda_{\min} = 300.0 \text{ nm}; \lambda_{\max} = 1800.0 \text{ nm}, \end{cases}$$

where $I(\tilde{\lambda})_{AM1.5}$ is the reference solar spectral irradiance and the normalized absorbance spectrum $\alpha(\tilde{\lambda})$ is deduced from the relation

$$\alpha(\tilde{\lambda}) = \frac{1}{d^{4/2}} \cdot \sqrt[4]{\left(\ln \frac{1-R(\tilde{\lambda})}{T(\tilde{\lambda})}\right)^4 + \left(2 \ln \frac{1-R(\tilde{\lambda})}{\sqrt{T(\tilde{\lambda})}}\right)^4}, \quad (22)$$

where d is the layer thickness. This parameter is used to classify certain semiconductor thin films along their absorption of light [54]. The calculated values of Ψ_{AB} of Ni-doped ZnO thin films are summarized in table 5. In addition, the decrease of this parameter Ni content from 19.7 to 1476×10^{-12} m 3 s $^{-1}$

Table 5. Values of the Amlouk–Boubaker opto-thermal expansivity Ψ_{AB} .

	Undoped ZnO	ZnO : Ni 2%	ZnO : Ni 3%	ZnO : Ni 4%
Ψ_{AB} (10^{-12} m ³ s ⁻¹)	19.7	15.8	14.53	14.76

is noted. This effect shows the incorporation of Ni doping in the ZnO matrix. This decrease in Ψ_{AB} is in good agreement with the decrease in the film transparency and the increase in the optical absorption of such doped films.

4. Conclusion

The structural and the optical properties of Ni-doped ZnO thin films deposited by the spray pyrolysis technique was investigated. The influence of Ni doping on the structural, PL, morphological and optical properties was presented. Structural characterization reveals that Ni ions are successfully incorporated into the ZnO lattice without any extra phase and wurtzite structure of ZnO is retained. All of Ni-doped ZnO films are highly transparent with a transmittance between 75 and 95% in the visible wavelength region. The high quality of the films is confirmed by the low value of the extinction coefficient. The optical band gap E_g of Ni-doped films exhibits a red shift.

In this study, the refractive-index dispersion was analysed using the single oscillator model. The Ni-doping affects the values of the calculated dispersion parameters such as oscillator energy, dispersion energy and oscillator strength. The results obtained by PL of sprayed ZnO thin films are discussed in terms of nickel content and it is found that they confirm those obtained by XRD. Finally, the behaviour of the dielectric constant components spectra needs more investigations particularly in infra-red region but beforehand that this result is quite encouraging since a costless and simple used depositing technique was considered.

References

- [1] Gupta R K, Ghosh K and Kahol P K 2010 *Mater. Lett.* **64** 1487
- [2] Kakeno T, Sakai K, Komaki H, Yoshino K, Sakemi H, Awai K, Yamamoto T and Ikari T 2005 *Mater. Sci. Eng. B* **118** 70
- [3] Hossain M M, Ku B-C and Hahn J R 2015 *Appl. Surf. Sci.* **354** 55
- [4] Neykova N, Hruska K, Holovsky J, Remes Z and Vanecek M 2013 *Thin Solid Films* **543** 110
- [5] Mhamdi A, Labidi A, Souissi B, Kahlaoui M, Yumak A, Boubaker K, Amlouk A and Amlouk M 2015 *J. Alloys Compd.* **639** 648
- [6] Han J, Gong H, Yang X, Qiu Z, Zi M, Qiu X, Wang H and Cao B 2015 *Appl. Surf. Sci.* **332** 549
- [7] Mahdhi H, Ben Ayadi Z, Gauffier J L, Djessas K and Alaya S 2015 *Opt. Mater.* **45** 97
- [8] Castro M V and Tavares C J 2015 *Thin Solid Films* **586** 13
- [9] Zaier A, Meftah A, Jaber A Y, Abdelaziz A A and Aida M S 2015 *J. King Saud Univ. — Sci.* **27** 356
- [10] Mhamdi A, Ouni B, Amlouk A, Boubaker K and Amlouk M 2014 *J. Alloys Compd.* **582** 810
- [11] Lee J-H, Ko K-H and Park B-O 2003 *J. Cryst. Growth* **247** 119
- [12] Omri K, El Ghoul J, Lemine O M, Bououdina M, Zhang B and El Mir L 2013 *Superlattices Microstruct.* **60** 139
- [13] Mhamdi A, Boukhachem A, Madani M, Lachheb H, Boubaker K, Amlouk A and Amlouk M 2013 *Optik* **124** 3764
- [14] Mhamdi A, Mimouni R, Amlouk A, Amlouk M and Belgacem S 2014 *J. Alloys Compd.* **610** 250
- [15] Mimouni R, Kamoun O, Yumak A, Mhamdi A, Boubaker K, Petkova P and Amlouk M 2015 *J. Alloys Compd.* **645** 100
- [16] Rajeh S, Mhamdi A, Khirouni K, Amlouk M and Guermazi S 2015 *Opt. Laser Technol.* **69** 113
- [17] Liu X X, Lin F T, Sun L L, Cheng W J, Ma X M and Shi W Z 2006 *Appl. Phys. Lett.* **88** 062508
- [18] Bodker F, Hansen M F, Koch C B and Morup S 2000 *J. Magn. Mater.* **221** 32
- [19] Yilmaz S, McGlynn E, Bacaksız E, Cullen J and Chellappan R K 2012 *Chem. Phys. Lett.* **525–526** 72
- [20] Cheng C W, Xu G Y, Zhang H Q and Luo Y 2008 *Mater. Lett.* **62** 1617
- [21] Ghosh S, Srivastava P, Pandey B, Saurav M, Bharadwaj P, Avasthi D K, Kabiraj D and Shivaprasad S M 2008 *Appl. Phys. A* **90** 765
- [22] Cong C J, Hong J H, Liu Q Y, Liao L and Zhang K L 2006 *Solid State Commun.* **138** 511
- [23] Wu D W, Yang M, Huang Z B, Yin G F, Liao X M, Kang Y Q, Chen X F and Wang H 2009 *J. Colloid Interface Sci.* **330** 380
- [24] Kim K H, Jin Z, Abe Y and Kawamura M 2015 *Mater. Lett.* **149** 8
- [25] Fang G, Li D and Yao B-L 2003 *J. Cryst. Growth* **247** 393
- [26] Boukhachem A, Ouni B, Karyauoui M, Madani A, Chtourou R and Amlouk M 2012 *Mater. Sci. Semicond. Proc.* **15** 282
- [27] Cullity B D 1978 *Elements of X-ray diffraction* (New York: Addison-Wesley Publishing Company)
- [28] Kaebler E F 1967 *Handbook of X-rays* (New York: McGraw-Hill)
- [29] Muniyandi I, Mani G K, Shankar P and Rayappan J B B 2014 *Ceram. Int.* **40** 7993
- [30] Zhang X, Li X M, Chen T L, Bian J M and Zhang C Y 2005 *Thin Solid Films* **492** 248
- [31] Castaneda L, Silva-Gonzalez R, Gracia-Jimenez J M, Hernandez-Torres M E, Avendano-Alejo M, Marquez-Beltran C, de la L Olvera M, Vega-Perez J and Maldonado A 2010 *J. Mater. Sci. Semicond. Process.* **13** 80
- [32] Mill G, Li Z G and Meisel D 1988 *J. Phys. Chem.* **92** 822

- [33] Ghazi M E, Izadifard M, Ghodsi F E and Yuonesi M 2011 *J. Super-Cond. Nov. Magn.* **25** 101
- [34] Patil S K, Shinde S S and Rajpure K Y 2013 *Ceram. Int.* **39** 3901
- [35] Ben Rabeh M and Kanzari M 2011 *Thin Solid Films* **519** 7288
- [36] Marquez E, Ramirez-Malo J B, Villares P, Jimenez-Garay R and Swanepoel R 1995 *Thin Solid Films* **254** 83
- [37] Swanepoel R 1983 *J. Phys. E: Sci. Instrum.* **16** 1214
- [38] Swanepoel R 1984 *J. Phys. E: Sci. Instrum.* **17** 896
- [39] Wemple S H and DiDomenico M 1971 *J. Phys. Rev. B* **3** 1338
- [40] DiDomenico M and Wemple S H 1969 *J. Appl. Phys.* **40** 720
- [41] Wemple S H 1973 *J. Phys. Rev. B* **7** 3767
- [42] Lee P A, Said G, Davis R and Lim T H 1969 *J. Phys. Chem. Solids* **30** 2719
- [43] Gervais F 2002 *Mater. Sci. Eng. R* **39** 29
- [44] Wolaton A K and Moss T S 1963 *Proc. R. Soc. A* **81** 5091
- [45] Omar M A 1993 *Elementary solid state physics* (New York: Addison-Wesley Publishing Company)
- [46] Belgacem S and Bennaceur R 1990 *Rev. Phys. Appl.* **25** 1245
- [47] Cho S, Ma J, Kim Y, Sun Y, Wong G K L and Ketterson J B 1999 *Appl. Phys. Lett.* **75** 2761
- [48] Ahmed F, Kumar S, Arshi N, Anwar M S and Koo B H 2012 *CrystEngComm* **14** 4016
- [49] Chen Z C, Zhug L J, Wu X M and Meng Y D 2007 *Thin Solid Films* **515** 5462
- [50] Kim K J and Park Y R 2004 *J. Appl. Phys.* **96** 4150
- [51] Zhao J, Hu L, Liu W and Wang Z 2007 *Appl. Surf. Sci.* **253** 6255
- [52] Kohan A F, Ceder G, Morgan D and Van de Walle C G 2000 *Phys. Rev. B* **61** 15019
- [53] Tabatabaei S, Zhao T, Awojoyogbe O and Moses F 2009 *Int. J. Heat Mass Transfer* **45** 1247
- [54] Fridjine S and Amlouk M 2009 *Phys. Lett. B* **23** 2179